Nuclear Materials and Energy 12 (2017) 536–540

Contents lists available at ScienceDirect

Nuclear Materials and Energy

journal homepage: www.elsevier.com/locate/nme

Remobilization of tungsten dust from castellated plasma-facing components

M. De Angeli[a], P. Tolias[b,*], S. Ratynskaia[b], D. Ripamonti[c], G. Riva[c], S. Bardin[d], T. Morgan[d], G. De Temmerman[e]

[a] Istituto di Fisica del Plasma - Consiglio Nazionale delle Ricerche, via Cozzi 53, 20125 Milan, Italy
[b] Space and Plasma Physics - KTH Royal Institute of Technology, Teknikringen 31, 10044 Stockholm, Sweden
[c] Institute of Condensed Matter Chemistry and Energy Technologies - Consiglio Nazionale delle Ricerche, via Cozzi 53, 20125 Milan, Italy
[d] FOM Institute DIFFER, Dutch Institute For Fundamental Energy Research, Eindhoven, The Netherlands
[e] ITER Organization, Route de Vinon-sur-Verdon, CS 90 046, 13067 St. Paul Lez Durance Cedex, France

ARTICLE INFO

Article history:
Received 12 June 2016
Revised 14 November 2016
Accepted 18 January 2017
Available online 9 March 2017

ABSTRACT

Studies of tungsten dust remobilization from castellated plasma-facing components can shed light to whether gaps constitute a dust accumulation site with important implications for monitoring but also removal. Castellated structures of ITER relevant geometry that contained pre-adhered tungsten dust of controlled deposition profile have been exposed in the Pilot-PSI linear device. The experiments were performed under steady state and transient plasma conditions, as well as varying magnetic field topologies. The results suggest that dust remobilization from the plasma-facing monoblock surface can enhance dust trapping in the gaps and that tungsten dust is efficiently trapped inside the gaps.

1. Introduction

In nuclear fusion installations such as ITER, dust monitoring activities are necessary to ensure that safety limits are not violated [1–3]. For a reliable estimate of the dust inventory, inspection needs to focus on in-vessel locations that have a high probability to sustain large dust concentrations. It is conventionally argued that gravity driven motion will tend to amass the dust grains at the floor of the vacuum vessel [4]. Such an assumption ignores adhesive interaction of dust with plasma-facing components (PFCs), which scales proportionally with its size and thus dominates the gravitational force by orders of magnitude already for micrometer metallic dust [5]. Consequently, alternative accumulation sites need to be considered. Theoretical predictions of their position are challenging, since they require the coupling of currently-incomplete dust / droplet generation models with dust transport codes.

In ITER, PFCs will be castellated in order to better withstand high thermomechanical stresses, *i.e.* split into small monoblock segments separated by thin – 0.5 mm wide – poloidal and toroidal gaps [6,7]. The gaps have the potential of constituting dust accumulation sites due to the shielding of their interior from intense plasma particle and heat fluxes [4]. This brings forth some unexplored issues. *(i) How can large amounts of W dust get trapped in the gaps?* Highly resolved measurements of W dust motion in the vicinity of castellated structures have revealed that, excluding the possibility of penetration, the presence of the gap does not otherwise affect dust trajectories in an observable manner [8]. Therefore, considering that the monoblock plasma-wetted area is much larger than the gap entrance area [9], simple geometrical arguments indicate that, for a uniform supply of dust, the largest fraction will be deposited on the top of the monoblocks. Hence, dust remobilization [5,10] from the top of the neighboring monoblocks can provide an important contribution to the dust population that is trapped inside the gaps provided that the detachment velocity has a strong tangential component, as indeed observed in Pilot-PSI experiments [5]. *(ii) How efficient is dust trapping inside the gaps?* Owing to the large adhesion strength of micron-sized grains, dust accumulation in the gaps will not be dominated by gravity. In ITER, the divertor targets are vertical so the gap bottom is perpendicular with respect to gravitational acceleration. Considering the edge plasma drifts and the well-documented dominance of the ion drag force in the dynamics [11], dust will be preferentially stuck on the vertical side of the toroidal gaps and thus exposed to stronger plasma. Hence, it is possible that trapped dust remobilizes and exits the gap under either steady state or transient plasma

* Corresponding author.
E-mail address: tolias@kth.se (P. Tolias).

http://dx.doi.org/10.1016/j.nme.2017.01.021

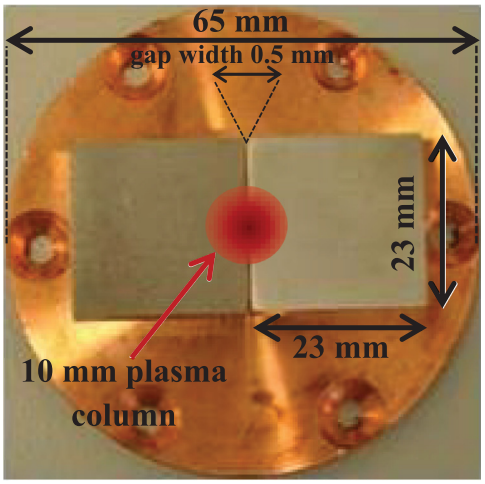

Fig. 1. The castellated W sample employed for normal plasma exposures with an indication of the Pilot-PSI column.

conditions. Moreover, the efficiency of gap trapping will also depend on the amount of dust residing in the gaps. Dust multilayer formation will weaken the adhesive forces and possibly facilitate remobilization. For completeness, we note that deposition of Be or seeding species in the gaps could also weaken adhesion.

In this work, we present the first experimental effort to address these questions. We report on Pilot-PSI experiments studying tungsten dust remobilization from castellated tungsten PFCs under both steady state and transient hydrogen plasma conditions and varying magnetic field topologies. We employ a recently proposed technique based on controlled pre-adhesion of dust grains on samples by gas dynamics methods and detailed scanning electron microscope (SEM) mapping of the deposition profiles prior to and post plasma exposure. The technique has already been implemented in a number of fusion devices but only planar W samples had been employed thus far [5,10]. Our results suggest that dust remobilization from the top of the monoblocks contributes to dust trapping in the gaps and indicate that tungsten dust is efficiently trapped in both the vertical sides and the bottom of the gaps.

2. Experimental set-up

2.1. Layout of the castellated samples

The experiments were performed with two different castellated sample layouts, one exposed perpendicularly and one exposed obliquely with respect to the incident plasma flow. The oblique exposures were characterized by ITER relevant magnetic field topology. However, in Pilot-PSI, for the formation of oblique angles between the sample surface and the axial magnetic field, it was necessary to employ a dedicated sample holder. This introduces the issue of properly aligning the plasma column with respect to the gap, or equivalently the issue of properly aligning the holder with respect to the device center.

The *samples exposed normal to the B-field* consisted of two non-chamfered W monoblocks $23 \times 23 \times 10$(h) mm^3 fixed on a common disk-shaped copper substrate. The gap width was 0.5 mm, the rms and arithmetic average measures of surface roughness were $R_q = 0.40\,\mu m$ and $R_a = 0.33\,\mu m$, respectively. The substrate was mounted directly at the plasma terminating surface of the chamber (endplate) implying that the B-field incidence was normal to the top side of the W blocks. The samples were arranged in a way that the plasma column was centred across the gap between the two monoblocks, as shown in Fig. 1.

The *samples exposed oblique to the B-field* consisted of a structure of four $23 \times 14 \times (6 - 5.5)$(h) mm^3 W monoblocks with a 0.5 mm gap width between each block, see the illustration presented in Fig. 2. The surface roughness measures were $R_q = 0.49\,\mu m$ and $R_a = 0.36\,\mu m$. The blocks were mounted on a rectangular copper support fixed to a graphite holder able to withstand the incident plasma heat load. The surface of the graphite holder was inclined by an angle of 3° with respect to the vessel axis. Moreover, the top surface of each monoblock was chamfered with an inclination angle of 1.2° with respect to the block base. Thus, the overall angle between the magnetic field and the top monoblock surface was 4.2°. The back side of the graphite holder was mounted on a disk-shaped molybdenum support fixed to the endplate during the experiments.

2.2. Types of dust deposition

Dust was pre-deposited by gas dynamic methods enabling control of the dust impact speed on the substrate, which needs to have values below the sticking threshold for adhesion to occur [12–14]. The deposition velocities for these experiments varied in the range $0.75 - 1.9\,ms^{-1}$. The use of circular and rectangular masks led to dust deposition profiles with sharp edges (dust spots) that facilitated an unambiguous interpretation of results. The deposition areas on the castellated structures have been mapped with SEM prior to and post plasma exposure and the resulting images have been overlapped to identify the dust remobilization activity. For a detailed description of the apparatus and the technique the reader is addressed to Ref. [5].

The W dust population was perfectly spherical with a nominal diameter in the $5 - 25\,\mu m$ range and >99.9% purity, supplied by TEKNA advanced materials. Dust was deposited on different regions of the castellated structures, namely on the top side of the monoblocks, on the vertical side of the gaps as well as on the bottom of the gaps. Two different deposition types were employed.

- *Type A deposition*: Dust was only adhered at the top side of the monoblocks, whereas the vertical and the bottom sides of the gaps were kept dust-free. The latter was accomplished by covering the gap with a protecting mask during dust deposition. Such a deposition pattern allowed us to study gap trapping induced by remobilization through the quantification of the amount of grains that were detached from the top-side and ended up in the gap interior.
- *Type B deposition*: Dust was adhered at the vertical and bottom sides of the gap, whereas the top side of the monoblocks was kept dust-free. Such a deposition pattern allowed us to study the gap trapping efficiency by identifying the amount of grains that escaped from the gap interior.

The dust spot locations, geometry and dimensions generally varied. They are depicted in Fig. 3 and summarized in the figure caption. We note that, in the oblique castellated structures, the dust deposition gap is located between the second and third monoblocks, see Fig. 2a the area marked with a blue circle.

2.3. Different plasma exposures

Pilot-PSI is a linear plasma device capable of producing ITER-divertor relevant plasma conditions. The plasma is generated by a cascaded arc source that exhausts into a 40 cm diameter vacuum vessel and is confined by a strong axial magnetic field [15]. The resulting plasma column is characterized by Gaussian radial density profiles with a full width at half maximum of about 10 mm. Pilot-PSI also allows the superposition of transient pulses to the steady state plasma [16,17] that can be comparable to ELM events

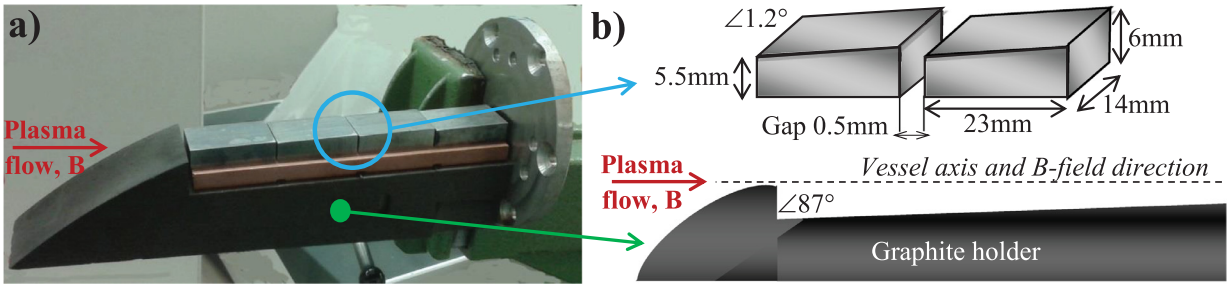

Fig. 2. The castellated W sample and the holder employed for oblique plasma exposures. (a) Photo of the four monoblock structure mounted on the graphite holder, the copper substrate and the molybdenum support are also visible. The blue circle indicates the location of the dust deposition area, between the second and third monoblocks. (b) A sketch of the W blocks and the graphite holder with their inclination with respect to the device axis and the magnetic field. (For interpretation of the references to colour in this figure legend, the reader is referred to the web version of this article.)

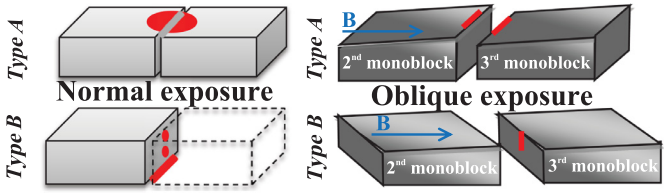

Fig. 3. Schematic representation of the different layouts of the castellated W samples together with the different types of dust deposition. The dust deposition areas (dust spots) are illustrated in red. For the Type A normal exposures (one sample), the top dust spot was circular with a 4 mm diameter, symmetrically placed with respect to the gap. For the Type B normal exposures (two samples), the two vertical dust spots were circular with a 1 mm diameter and the bottom dust spot was rectangular 0.5 × 4 mm^2. For the Type A oblique exposures (three samples), the two top dust spots were rectangular 0.5 × 4 mm^2. For the Type B oblique exposures (three samples), the vertical dust spot was rectangular 0.5 × 4 mm^2. (For interpretation of the references to colour in this figure legend, the reader is referred to the web version of this article.)

expected in ITER in terms of the mean energy per unit area deposited on the target and the repetition rate. All castellated samples were mounted on the electrically floating endplate. A 2D infrared (IR) camera FLIR SC7500-MB was viewing directly the top side of the monoblocks. For the normal exposures, the electron density n_e and electron temperature T_e were measured 17 mm in front of the endplate, by means of a Thomson Scattering (TS) system [18], in discharges with the same input parameters but with a planar dust-free endplate. The sample holder for the oblique exposures blocks the path for the TS laser, making TS measurements impossible in such a configuration.

Samples exposed normal to the B-field under steady state plasma conditions. The first set of three castellated samples (one Type A, two Type B) was exposed to single identical steady state discharges of 2 s plateau duration with current $I = 190$ A, magnetic field $B = 0.8$ T and 2.75 slm (standard liters per minute) hydrogen gas flow. The plasma density and electron temperature at the centre of the column were $n_e = 6 \times 10^{20}$ m^{-3} and $T_e = 1.1$ eV yielding a 0.3 μm Debye length that is much smaller than the gap width. The surface temperature close to the gap edge was ~550 °C.

Samples exposed oblique to the B-field under ELM-like plasma conditions. Two castellated samples (one Type A, one Type B) were exposed to a single $\Delta\tau = 1$ ms ELM-like pulse. The ELM-like discharges were achieved by superimposing a $V_{ch} = 1800$ V voltage to the plasma source, by means of bank capacitors, during background steady state discharges with $I = 190A$, $B = 1.6$ T and 7 slm H_2 gas flow. Four castellated samples (two Type A, two Type B), were exposed to ten $\Delta\tau = 1$ ms consecutive ELM-like pulses with a 10 Hz repetition rate and $V_{ch} = 1800$ V. The background settings were $I = 240$ A, $B = 1.6$ T and 6 slm H_2 gas flow. At the end of the discharge, the surface temperature, close to the gap edge and at the center of the dust spot, reached ~1150 °C. For the latter discharge settings, the heat flux recovered from IR measurements with the planar perpendicular endplate had a pulse-average value of ~700 MW/m^2 at the center of the column. Employing the optical approximation for the incident angle of 4.2°, we acquire $q_\perp = 50$ MW/m^2 for the normal flux received by the top of the blocks, see Ref. [10] for details.

3. Results and discussion

Samples exposed normal to the B-field. Analysis of the Type A sample revealed that remobilization activity took place mostly in the top monoblock areas closest to the gap edges. Given the Gaussian decaying plasma profiles inside the column and the presence of the 0.5 mm wide gap, this is merely a consequence of the stronger local plasma-dust interaction. When only taking into account the spot area within 1 mm away from the gap edge, the remobilization rate is ~30%: the majority of the detached grains were either clusters or large grains at the tail of the size distribution, in accordance with the scalings discussed in details in Ref. [5]. An example of remobilization activity close to the edge is shown in Fig. 4, where the gap is also identified and so are the positions of the detached grains. Moreover, few of the grains originally residing very close to the gap edge have been displaced in the gap interior. By comparing the SEM images of the top and vertical sides prior to and post exposure, it is possible to identify their final location. In Fig. 5 we demonstrate how such an identification is possible. We emphasize that the 90° transition between the top side and the vertical side of the monoblock is not sharp but gradual due to the non-zero local surface curvature. As a consequence, the gap edge is essentially a strip that is several tens of micrometers wide (the width differs between the castellated samples). Analysis of the Type B samples revealed no dust grains emerging on the top-side of the monoblocks, in spite of the fact that in one of these samples dust multilayers were deposited at the gap bottom. This indicates that gap trapping is efficient - none of the dust residing on the side and bottom surface was released during the exposures.

Samples exposed oblique to the B-field. The Type A sample exposed to a single ELM-like pulse exhibited no remobilization activity. On the other hand, in the Type A samples exposed to multiple repetitive ELM-like pulses remobilization took place on both the upstream and shadowed edges, ~20% of the grains got detached. Figs. 6 and 7 illustrate examples for the upstream and shadowed monoblocks, respectively. The difference between the number of dust grains close to the edges prior to and post exposure is easily observable on both figures. However, away from the edges, the remobilization activity was much lower (see Figs. 6 and 7), again

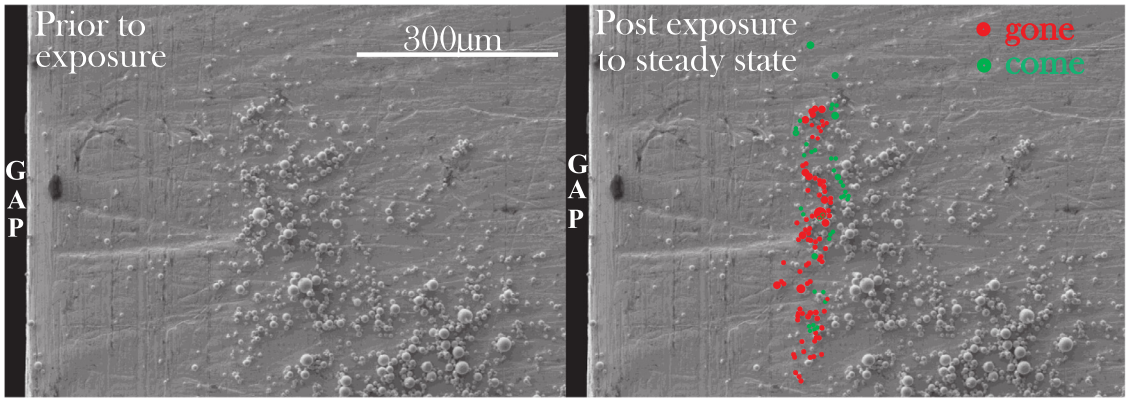

Fig. 4. Remobilization during the normal exposure of Type A castellated samples. SEM images of the dust deposition area that lies in the proximity of the gap, prior to and post exposure to the steady state Pilot-PSI plasma. The remobilization activity is confined to an ellipsoidal area located very close to the gap. The color coding is as follows: dust grains that were removed from their initial position and whose terminal position is not clear are coded by red, dust grains that appeared after plasma exposure and whose initial position is not clear are coded by green. (For interpretation of the references to colour in this figure legend, the reader is referred to the web version of this article.)

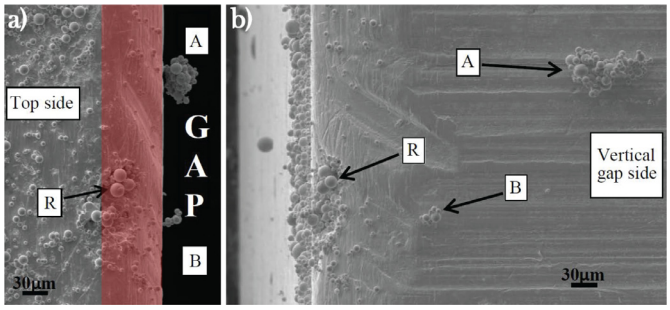

Fig. 5. Normal exposure of Type A castellated samples; identification of the final location of remobilized dust grains that were displaced in the gap interior. SEM images of the top (deposition area) and vertical side (initially dust-free) post exposure to the steady state Pilot-PSI plasma. The red strip designates the monoblock edge, since the top–to–vertical transition is not sharp due to the non-zero local surface curvature. A reference cluster "R" can be distinguished in both views as well as two large clusters "A" and "B" residing about 100 and 300 μm deep in the vertical side of the gap. (For interpretation of the references to colour in this figure legend, the reader is referred to the web version of this article.)

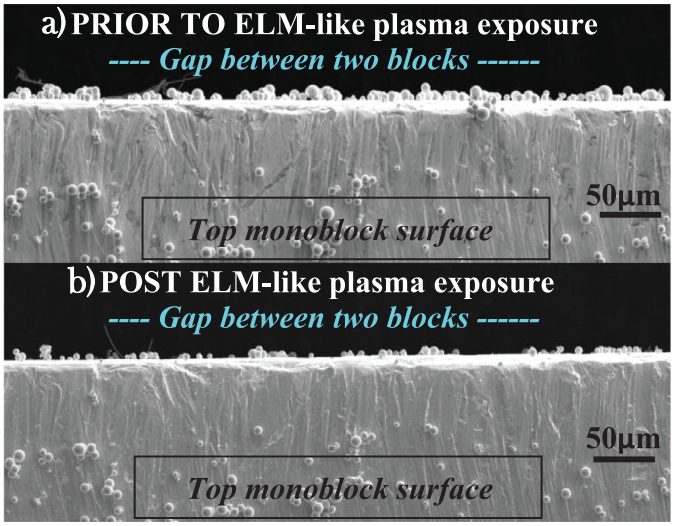

Fig. 6. Remobilization during the oblique exposure of Type A castellated samples. SEM images of the **upstream edge** dust spot, prior to and post exposure to repetitive ELM-like Pilot-PSI pulses.

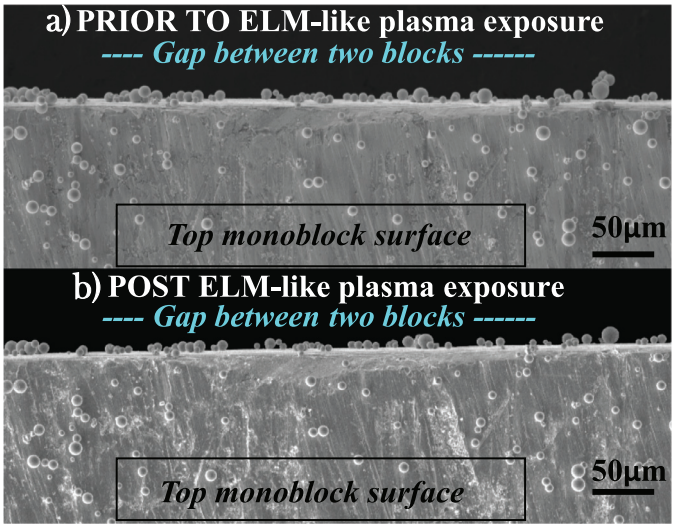

Fig. 7. Remobilization during the oblique exposure of Type A castellated samples. SEM images of the **shadowed edge** dust spot, prior to and post exposure to repetitive ELM-like Pilot-PSI pulses.

owing to the rapid spatial decay of the plasma density and temperature away from the column center. Post exposure, an appreciable amount of dust was detected on the vertical sides of the gaps of these Type A samples. The most probable location is several hundred micrometers deep, but some grains were detected as far as 3.5 mm away from the edge. Moreover, on each sample, the remobilized grains resided deeper on the vertical side of the upstream monoblock as compared to the vertical side of the shadowed monoblock. Finally, a few instances of molten clusters and wetting induced coagulation have been observed on these samples [10]. Analysis of the Type B samples, exposed to both single and multiple ELM-like pulses, revealed a behaviour similar to the normally exposed samples; nearly no dust was found on the top surfaces.

Reference samples. In order to ensure that the observed dust remobilization was not due to the sample transportation, endplate mounting or exposure to the background pre-ELM plasma, two samples (one of each type), have been handled in the same manner but exposed only to the background plasma (and not to the plasma with superimposed ELM-like pulses). SEM revealed no remobilization activity in neither of them.

4. Conclusions

Castellated W samples of ITER relevant geometry containing pre-adhered W dust were exposed to the Pilot-PSI plasma, perpendicularly and obliquely with respect to the magnetic field under steady-state and ELM-replicating conditions. The results of these exposures can be summarized in the following: (i) Dust is efficiently trapped inside the gaps. W dust grains adhered either at the vertical side or at the bottom of the gap, were almost never removed from the gap interior even during the interaction with repetitive ELMs. (ii) An appreciable, ~20%, remobilization activity was observed at the gap edges in the case of repetitive ELMs in oblique exposures. The majority of W dust that remobilized from the top edge of the monoblocks ended up residing on the vertical sides of the gap, which suggests that remobilization from adjacent monoblocks could contribute to dust accumulation in the gaps.

We emphasize again that in Pilot-PSI the mounting of the oblique castellated structures requires the use of external mechanical support, which unavoidably brings forth alignment issues. Therefore, it would be valuable to verify the current conclusions by performing similar oblique exposures in Magnum-PSI. There, the endplate orientation with respect to the magnetic field can be adjusted at various angles without the need to introduce an external holder [19].

Acknowledgments

This work has been carried out within the framework of the EUROfusion Consortium and has received funding from the Euratom research and training programme 2014–2018 under grant agreement No 633053. Work performed under EUROfusion WP PFC. The views and opinions expressed herein do not necessarily reflect those of the European Commission and the ITER Organization.

References

[1] S. Rosanvallon, C. Grisolia, P. Delaporte, J. Worms, et al., J. Nucl. Mater. 882 (2009) 386–388.
[2] C.-H. Choi, A. Tesini, R. Subramanian, A. Rolfe, et al., Fus. Eng. Des. 1448 (2015) 98–99.
[3] R. Reichle, P. Andrew, P. Bates, O. Bede, et al., J. Nucl. Mater. 180 (2015) 463.
[4] M. Shimada, R.A. Pitts, S. Ciattaglia, S. Carpentier, et al., J. Nucl. Mater. S996 (2013) 438.
[5] P. Tolias, S. Ratynskaia, M. De Angeli, G. De Temmerman, et al., Plasma Phys. Control. Fus. 025009 (2016) 58.
[6] R.A. Pitts, S. Carpentier, F. Escourbiac, T. Hirai, et al., J. Nucl. Mater. S48 (2013) 438.
[7] S.C. Chouchana, T. Hirai, F. Escourbiac, A. Durocher, et al., Phys. Scr. 014002 (2014) T159.
[8] A. Shalpegin, F. Brochard, S. Ratynskaia, P. Tolias, et al., Nucl. Fus. 112001 (2015) 55.
[9] J. Roth, E. Tsitrone, A. Loarte, T. Loarer, et al., J. Nucl. Mater. 1 (2009) 390–391.
[10] S. Ratynskaia, P. Tolias, I. Bykov, D. Rudakov, et al., Nucl. Fus. 066010 (2016) 56.
[11] S.I. Krasheninnikov, R.D. Smirnov, D.L. Rudakov, Plasma Phys. Control. Fus. 083001 (2011) 53.
[12] S. Ratynskaia, C. Castaldo, H.B. ker, D. Rudakov, Plasma Phys. Control. Fus. 074009 (2011) 53.
[13] S. Ratynskaia, L. Vignitchouk, P. Tolias, I. Bykov, et al., Nucl. Fus. 123002 (2013) 53.
[14] L. Vignitchouk, P. Tolias, S. Ratynskaia, Plasma Phys. Control. Fus. 095005 (2014) 56.
[15] G.J. van Rooij, V.P. Veremiyenko, W.J. Goedheer, B. de Groot, et al., Appl. Phys. Lett. 121501 (2007) 90.
[16] G. De Temmerman, J.J. Zielinski, S. van Diepen, L. Marot, M. Price, Nucl. Fus. 073008 (2011) 51.
[17] T.W. Morgan, T.M. de Kruif, H.J. van der Meiden, M.A. van den Berg, et al., Plasma Phys. Control. Fus. 095004 (2014) 56.
[18] H.J. van der Meiden, R.S. Al, C.J. Barth, A.J.H. Donné, et al., Rev. Sci. Instrum. 013505 (2008) 79.
[19] G. De Temmerman, M.A. van den Berg, J. Scholten, A. Lof, et al., Fus. Eng. Des. 483 (2013) 88.